

Physics package based on intracavity laser cooling ^{87}Rb atoms for space cold atom microwave clock

Siminda Deng(邓思敏达), Wei Ren(任伟), Jingfeng Xiang(项静峰), Jianbo Zhao(赵剑波), Lin Li(李琳), Di Zhang(张迪), Jinyin Wan(万金银), Yanling Meng(孟艳玲), Xiaojun Jiang(蒋小军), Tang Li(李唐), Liang Liu(刘亮), and Desheng Lü(吕德胜)

Citation: Chin. Phys. B, 2024, 33 (**7**): 070602. DOI: 10.1088/1674-1056/ad4bc1
Journal homepage: http://cpb.iphy.ac.cn; http://iopscience.iop.org/cpb

What follows is a list of articles you may be interested in

Proposal for a realtime Einstein-synchronization-defined satellite virtual clock

Chenhao Yan(严晨皓), Xueyi Tang(汤雪逸), Shiguang Wang(王时光), Lijiaoyue Meng(孟李皎悦), Haiyuan Sun(孙海媛), Yibin He(何奕彬), and Lijun Wang(王力军)
Chin. Phys. B, 2024, 33 (**7**): 070601. DOI: 10.1088/1674-1056/ad3dc9

A Yb optical clock with a lattice power enhancement cavity

Chunyun Wang(王春云), Yuan Yao(姚远), Haosen Shi(师浩森), Hongfu Yu(于洪浮),Longsheng Ma(马龙生), and Yanyi Jiang(蒋燕义)
Chin. Phys. B, 2024, 33 (**3**): 030601. DOI: 10.1088/1674-1056/ad1986

Effective sideband cooling in an ytterbium optical lattice clock

Jin-Qi Wang(王进起), Ang Zhang(张昂), Cong-Cong Tian(田聪聪), Ni Yin(殷妮), Qiang Zhu(朱强), Bing Wang(王兵), Zhuan-Xian Xiong(熊转贤), Ling-Xiang He(贺凌翔), and Bao-Long Lv(吕宝龙)
Chin. Phys. B, 2022, 31 (**9**): 090601. DOI: 10.1088/1674-1056/ac5392

Study of optical clocks based on ultracold ^{171}Yb atoms

Di Ai(艾迪), Hao Qiao(谯皓), Shuang Zhang(张爽), Li-Meng Luo(骆莉梦), Chang-Yue Sun(孙常越), Sheng Zhang(张胜), Cheng-Quan Peng(彭成权), Qi-Chao Qi(齐启超), Tao-Yun Jin(金涛韫), Min Zhou(周敏), Xin-Ye Xu(徐信业)
Chin. Phys. B, 2020, 29 (**9**): 090601. DOI: 10.1088/1674-1056/aba099

Analysis of iris-loaded resonance cavity in miniaturized maser

Zu-Gen Guo(郭祖根), Yong Zhang(张勇), Tao Tang(唐涛), Zhan-Liang Wang(王战亮), Yu-Bin Gong(宫玉彬), Fei Xiao(肖飞), Hua-Rong Gong(巩华荣)
Chin. Phys. B, 2020, 29 (**5**): 050601. DOI: 10.1088/1674-1056/ab7d98

INSTRUMENTATION AND MEASUREMENT

Physics package based on intracavity laser cooling ^{87}Rb atoms for space cold atom microwave clock

Siminda Deng(邓思敏达)[1,2,3], Wei Ren(任伟)[1,2,3,†], Jingfeng Xiang(项静峰)[1,2], Jianbo Zhao(赵剑波)[1,2], Lin Li(李琳)[1,2,3], Di Zhang(张迪)[1,2], Jinyin Wan(万金银)[1,2,3], Yanling Meng(孟艳玲)[1,2,3], Xiaojun Jiang(蒋小军)[1,2], Tang Li(李唐)[1,2,3], Liang Liu(刘亮)[1,2,3], and Desheng Lü(吕德胜)[1,2,3,‡]

[1] *Aerospace Laser Technology and System Department, Shanghai Institute of Optics and Fine Mechanics, Chinese Academy of Sciences, Shanghai* 201800, *China*

[2] *Key Laboratory of Quantum Optics, Shanghai Institute of Optics and Fine Mechanics, Chinese Academy of Sciences, Shanghai* 201800, *China*

[3] *Center of Materials Science and Optoelectronics Engineering, University of Chinese Academy of Sciences, Beijing* 100049, *China*

(Received 18 April 2024; revised manuscript received 6 May 2024; accepted manuscript online 15 May 2024)

This article proposes a new physics package to enhance the frequency stability of the space cold atom clock with the advantages of a microgravity environment. Clock working processes, including atom cooling, atomic state preparation, microwave interrogation, and transition probability detection, are integrated into the cylindrical microwave cavity to achieve a high-performance and compact physics package for the space cold atom clock. We present the detailed design and ground-test results of the cold atom clock physics package in this article, which demonstrates a frequency stability of $1.2\times10^{-12}\ \tau^{-1/2}$ with a Ramsey linewidth of 12.5 Hz, and a better performance is predicted with a 1 Hz or a narrower Ramsey linewidth in microgravity environment. The miniaturized cold atom clock based on intracavity cooling has great potential for achieving space high-precision time-frequency reference in the future.

Keywords: atomic clock, microgravity, microwave cavity, space station, frequency stability

PACS: 06.30.Ft, 91.10.Fc, 43.58.Hp, 95.55.Sh **DOI:** 10.1088/1674-1056/ad4bc1

1. Introduction

High-performance atomic clocks, when operating in the orbit of satellites, are pivotal for fundamental physics research,[1,2] deep space exploration,[3] and global navigation and positioning.[4] Cold atom clocks offer potential advantages in frequency stability and uncertainty compared with traditional atomic clocks.[5,6] Consequently, there is an ongoing effort to develop cold atom clocks for space satellite platforms. The Cold Atom Clock Experiment in Space (CACES), which utilizes laser-cooled rubidium atoms, was launched into the Chinese space laboratory Tiangong-2 in 2016.[7] The long-term operation of CACES in orbit paves the way for the application of space-based cold atom clocks.[8,9] The Projet d'Horloge Atomique par Refroidissement d'Atomes en Orbite (PHARAO), developed by CNES,[10] serves as the primary instrument of the Atomic Clock Ensemble in Space (ACES).[11] PHARAO has successfully completed ground tests and is scheduled for launch to the International Space Station (ISS) in 2025.[12] The ACES mission will perform an absolute measurement of the redshift effect between the PHARAO clock on-board the International Space Station and clocks on Earth, improving this limit by an order of magnitude.

This article introduces a new type of space cold atom clock physics package, utilizing intracavity laser cooling. We have constructed a three-dimensional optical molasses at the center of a cylindrical microwave cavity, which resonated with the ^{87}Rb clock transition frequency. Intense cold atomic beams from a low-velocity intense source (LVIS)[13] are captured by the molasses.[14] Subsequently, these cold atoms undergo a series of clock processes within the microwave cavity, including state selection, Ramsey interrogation, and state detection.[15] Integrating all these clock processes into a cylindrical TE011 mode microwave cavity facilitates the miniaturization of the space cold atom clock. Furthermore, when the clock operates in space, the microgravity environment allows the cold atoms to interact with the microwaves *in situ* for an extended period, thereby enhancing the clock frequency stability.[2,16] As part of the CACES follow on project, the cold atom microwave clock, based on the intracavity cooling of ^{87}Rb atoms, will be operated with an optical lattice clock and a hydrogen maser on-board the China Space Station. The atomic clock ensemble in the space station will integrate the characteristics of cold atom microwave clock, optical lattice clock, and hydrogen maser to build an ultra-high precision time frequency system, and carry out relevant physics experiments and applications.

This article illustrates the integration of reliable laser cooling and detection optics, in conjunction with cold atomic

†Corresponding author. E-mail: renweimiao87@siom.ac.cn
‡Corresponding author. E-mail: dslv@siom.ac.cn

© 2024 Chinese Physical Society and IOP Publishing Ltd

beams, into a high quality factor microwave cavity. We further present the design of a compact LVIS alongside the configuration of the vacuum chamber and magnetic shields to fulfill the prerequisites for high-performance atomic clocks. Ground-test results indicate that 5×10^7 ^{87}Rb cold atoms at an approximate temperature of 5 μK were successfully captured within the microwave cavity. By locking the microwave local oscillator frequency at the center of the Ramsey fringes, which have a width of 12.5 Hz, the output signal from the atomic clock achieved a frequency stability of $1.2\times10^{-12}\ \tau^{-1/2}$. The entire physics package retained its initial performance in the following mechanical vibration and thermal cycling tests.

2. Design of physics package

The comprehensive physics package sectional view of the space cold atom clock is depicted in Fig. 1. The central crossed vacuum tube branches the physics package into 3 parts. The first part on the right side contains an ion pump with a pumping speed of 20 L/S, which maintains a pressure of 10^{-8} Pa in the main vacuum chamber. The second part comprises the LVIS structure beneath the crossed vacuum tube, shielded by a two-layer permalloy cube magnetic shield. A differential pumping tube, with a diameter of 2 mm and a length of 12.5 mm, connects the LVIS vacuum chamber to the main vacuum tube. This connection ensures that the vacuum pressure in the LVIS chamber remains 1–2 orders of magnitude higher than that in the main chamber, guaranteeing an adequate background pressure of ^{87}Rb atoms within the 2D laser cooling zone. In the final part, the main vacuum chamber, positioned above the crossed vacuum tube, is shielded by five layers of cylindrical permalloy magnetic shields.

A 3D molasses is constructed in a microwave cavity inside the vacuum chamber to capture the cold atomic beam leaking from the LVIS. Subsequently, these cold atoms are manipulated in the microwave cavity and complete an atomic clock cycle. Different from the previous approaches by Liu *et al.*[17] and Esnault *et al.*,[18] which focused on compact atomic clocks utilizing intracavity isotropic laser cooling, as well as Müller *et al.*[19] and Lee *et al.*[20] who employed intracavity magneto-optical traps, the integration of 3D and LVIS for intracavity cooling in atomic clocks offers the advantage of achieving rapid sub-Doppler cooling of cold atoms without compromising the microwave cavity due to stray magnetic field interference.

The LVIS vacuum chamber has a cuboid shape measuring approximately 60 mm × 60 mm × 70 mm. Among the six faces of the cube, only the face connected to the main vacuum tube with a $\Phi = 62$ mm flange does not have a 25 mm diameter aperture window mounted on it. Three 25 mm $1/e^2$ diameter collimated laser sources are installed on the three perpendicular surfaces of the cube, with an average laser intensity of approximately 4 mW/cm^2 per beam. Three pairs of counterpropagating laser beams are formed by reflecting three laser beams with retroreflecting optics elements. Each retroreflecting optics element consists of a quarter-wave plate and a mirror. The six cooling laser beams and a pair of anti-Helmholtz coils form an LVIS region.[13,21] Two 2 mm diameter holes were drilled in the center of the wave plate and reflector facing the 3D chamber to extract the atomic beam from the MOT trapping region. And then the low velocity atomic beam flies into the center of the 3D molasses along the vacuum tube. A Rb source is installed on one of the edges of the cube structure. The overall size of the LVIS, including the anti-Helmholtz coils and laser source, is approximately 152 mm × 152 mm × 164 mm.

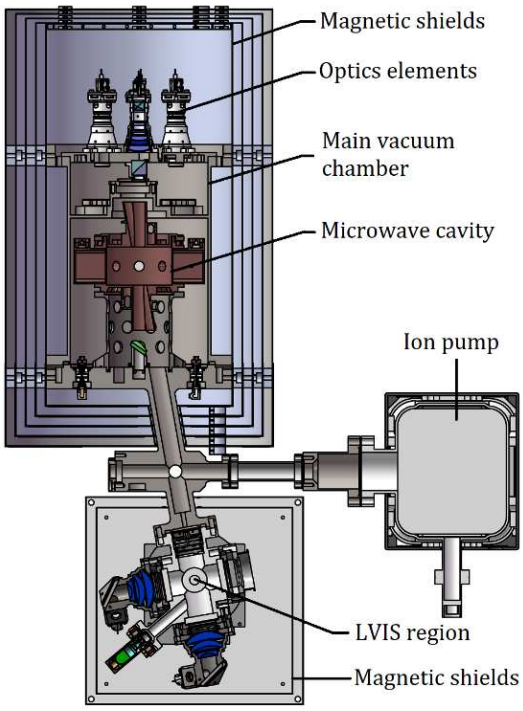


Fig. 1. Sectional view of the physics package for cold atom microwave clock. The physics package consists of magnetic shields, a main vacuum chamber, an LVIS region, and an ion pump.

The main vacuum chamber houses an oxygen-free copper material microwave cavity, operating in TE011 mode. This cavity resonates with the transition frequency between the hyperfine energy levels of ^{87}Rb atoms' ground states, which split at 6.834 GHz. In addition to an ion pump, four passive getter pumps are incorporated within the vacuum chamber. These pumps collectively achieve a total pumping speed of 48 L/s, ensuring the maintenance of vacuum pressure even when the power supply is disconnected.[22]

As shown in Fig. 2, the microwave cavity primarily comprises a top cover, a bottom cover, and a cylindrical cavity body in the middle. At the center of each cover lies a cutoff waveguide, 60 mm in length and 12 mm in inner diameter, designed to introduce cooling laser beams in the Z-direction while preventing perturbation of microwave power. Additionally, both covers feature an 8 mm diameter cutoff waveguide,

offset by 10° from the central cutoff waveguide and utilized for introducing cold atomic beams from the LVIS. There are eight evenly spaced apertures located around the microwave cavity, used for feeding microwave power, introducing cooling lasers, and collecting fluorescence.

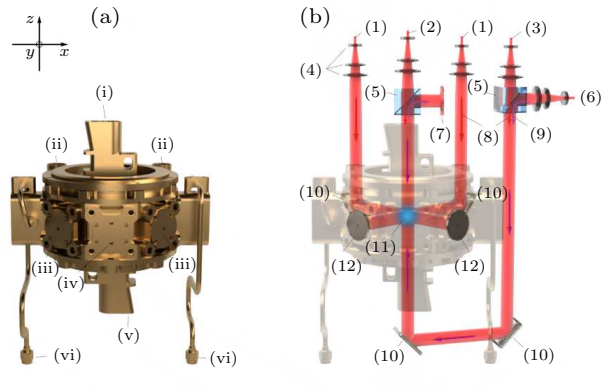


Fig. 2. Principle of intracavity cooling. (a) Structure of the microwave cavity. (b) Laser beam path diagram at the microwave cavity. (i) Cut-off waveguide, (ii) side cut-off waveguides, (iii) waveplate and reflectors, (iv) fluorescence collection photodiodes, (v) LVIS atomic channel, (vi) microwave feed-in. (1) Transverse cooling lasers, (2) downward cooling laser, (3) upward cooling laser, (4) extender lens set, (5) polarization beam splitter, (6) detecting laser, (7) 0° reflector, (8) cooling laser direction, (9) detecting laser direction, (10) 45° reflectors, (11) atomic cloud, (12) combination of waveplate and reflectors.

In Fig. 2, the cavity features symmetrical power-feeding holes in the X-axis directions, each with a diameter of 6 mm. Microwave power is channeled into the rectangular waveguide via the outer coaxial line and subsequently into the microwave cavity through these 6 mm holes. This symmetrical feeding arrangement effectively minimizes microwave phase variations in the cavity, mitigating distributed cavity phase errors in the cold atom clock.[23,24] Two symmetrical photodiodes with a surface dimension of 10 mm × 10 mm are positioned on the cavity along the Y-axis direction to capture cold atomic fluorescence. The dual photodiode arrangement serves as a backup for each other and enhances fluorescence collection efficiency. Adjacent to the X and Y axes at a 45° angle, four 10 mm diameter apertures in the cavity are designed to introduce two transverse cooling laser beams and retroreflectors on the opposite side. Remarkably, despite these apertures, the microwave cavity maintains a Q value exceeding 5000.

Laser beams are introduced into the microwave cavity through the top window of the vacuum chamber. Two transverse laser beams in the cavity from the top are incident from the cut-off waveguide on the side and then reflected into the microwave cavity by a 45° reflector. Two independent laser beams propagate in the opposite direction along the Z-axis, aiming to generate a traveling wave field in the microwave cavity during the detection process. During ground testing, two independent laser beams can also form a moving optical molasses to launch the atomic cloud at a certain height and prolong the interaction time between the atoms and microwaves.

The detection laser beam is concurrently superimposed with a cooling laser beam in the Z direction, utilizing a polarization beam splitter (PBS). Upon traversing a quarter-wave plate, these two laser beams transition from perpendicular linearly polarized to left-circularly polarized and right-circularly polarized, respectively. When the detection laser beam emerges from another PBS, it is reflected by a mirror, forming a standing wave within the cavity and enhancing the atomic photon scattering rate. Each cooling beam possesses an average laser intensity of approximately 25 mW/cm^2 and a $1/e^2$ diameter of 9 mm. The cross-section of the cooling laser beams at the microwave cavity's center dictates the size of the cold atoms' capture region. In both the transverse cooling beams and the detection beam, alongside the cooling laser with a frequency red detuned from the $F = 2 \rightarrow F' = 3$ transitions, there are also lasers with a frequency resonant with another transition $F = 1 \rightarrow F' = 2$, referred to as repumping lasers.

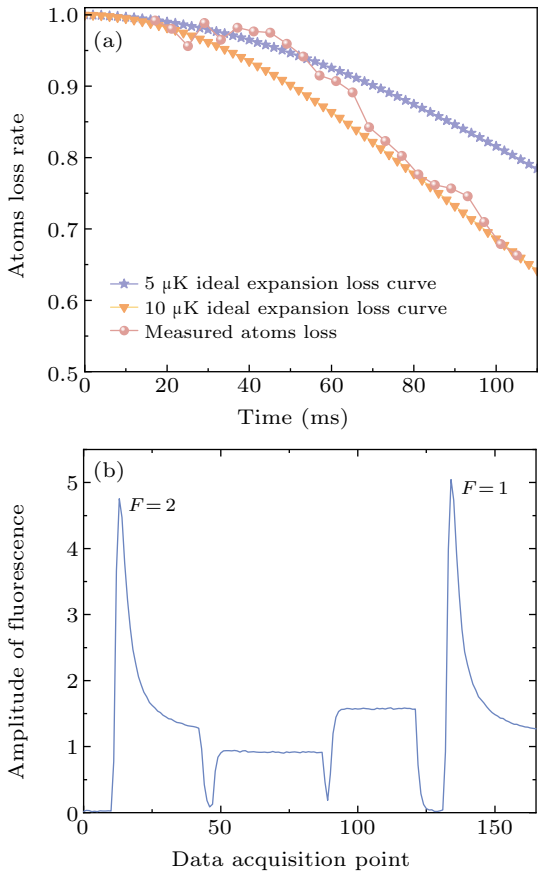


Fig. 3. (a) Results of cold atoms temperature testing. After 50 ms, the fluorescence collection efficiency decreases due to the fall of the atomic cloud. (b) The fluorescence signal of the cold atom cloud after the selection and interrogation stage with the double-level detection method. There are two peaks on the curve representing the atoms in $F = 2$ and $F = 1$, respectively. The two platforms on the curve, on behalf of the pushing laser beam and the repumping laser beam, turn on at the moment sequentially.

The distance between the center of the LVIS and the center of the microwave cavity is approximately 310 mm. The

molasses has the capacity to capture 5×10^7 atoms from a low-velocity atomic beam in 0.5 s. Following polarization gradient cooling, the temperature of the cold atomic cloud was assessed using the time-of-flight (TOF) method, and the result of this test is depicted in Fig. 3(a). A comparison of the decay curve of the detected number of cold atoms released from the molasses with the ideal atomic cloud expansion loss curve under a vacuum pressure of 10^{-8} Pa allows us to infer that the temperature of the cold atom cloud approximates 5 μK upon release from the optical molasses.

3. Performance of physics package

In the operation of the atomic clock, three LVIS laser beams, four 3D cooling laser beams, one detection laser beam, and the repump components superimposed within these beams can be independently regulated by the AOMs and mechanical shutters. Figure 4 illustrates the power control of each beam in every clock cycle. The coordination of these laser manipulations with the control of microwave signals and fluorescence detection facilitates the completion of the entire atomic clock cycle.

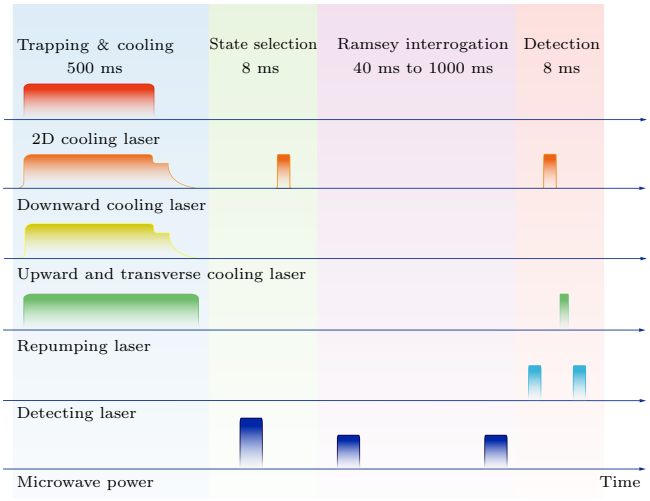


Fig. 4. Time sequence of laser beams and microwave power in a single clock cycle of cold atom microwave clock.

In the sequence of clock cycles depicted in Fig. 4, cold atoms released from the molasses uniformly populate all five Zeeman sublevels of the ground state $F=2$. We employ a π-pulse microwave to excite atoms in the $|F=2,m_F=0\rangle$ state to the $|F=1,m_F=0\rangle$ state. Subsequently, atoms in other Zeeman sublevels of $F=2$ are pushed away by the traveling laser in Z direction. The atoms remaining in the $|F=1,m_F=0\rangle$ state will then undergo two Ramsey $\pi/2$ microwave pulses. These pulses induce a quantum superposition state for all atoms between $|F=1,m_F=0\rangle$ and $|F=2,m_F=0\rangle$, with the transition probability being contingent on the disparity between the microwave frequency and the clock transition frequency. Populations of both atomic states, $|F=2,m_F=0\rangle$ and $|F=1,m_F=0\rangle$ (N_2 and N_1), are identified using the double-level detection method, as depicted in Fig. 3(b). Analysis of the fluorescence signal suggests that each of these two quantum states contains approximately 4×10^6 atoms. The normalized transition probability from $|F=1,m_F=0\rangle$ to $|F=2,m_F=0\rangle$ is calculated from $N_2/(N_1+N_2)$, and the difference between the microwave frequency and atomic transition frequency is subsequently computed.

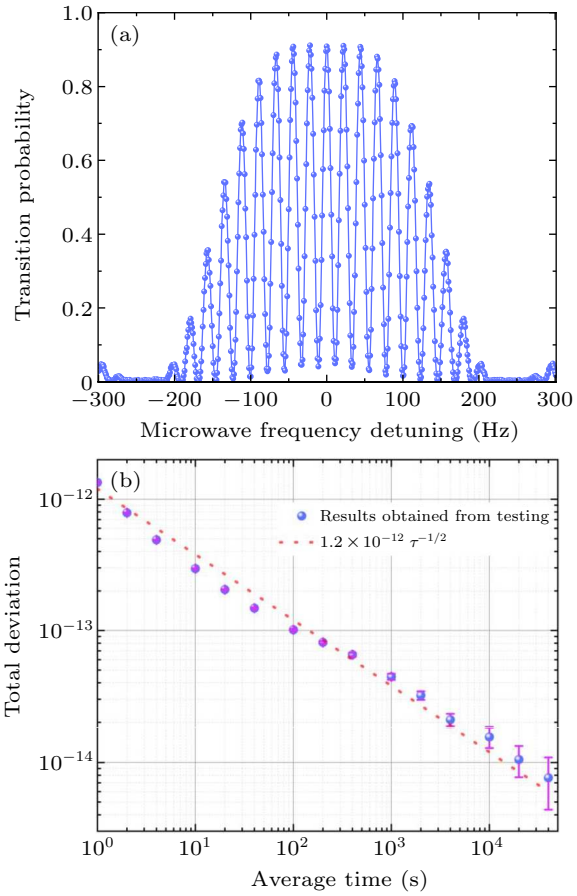


Fig. 5. (a) Ramsey fringes obtained by scanning the microwave frequency detuning. (b) The output frequency Alain deviation of the cold atom microwave clock. Segment line: the situation with a frequency stability of $1.2\times10^{-12}\ \tau^{-1/2}$.

Figure 5(a) illustrates the Ramsey fringes derived from scanning the microwave frequency. These fringes depict the variation in the transition probability of atoms as we adjust the microwave frequency detuning relative to the clock frequency. The stability of the atomic clock's frequency can be ascertained through the signal-to-noise ratio and linewidth of the Ramsey fringes. The primary noise affecting the transition probability is comprised of quantum projection noise, detection noise, and microwave local oscillator noise.[25,26] In our experimental setup, the dominant noise originates from the detection system, yielding Ramsey fringes with a signal-to-noise ratio of approximately 500, as depicted in Fig. 5(a). The line width of the central peak within these Ramsey fringes measures about 12.5 Hz, correlating to a time interval of 40 ms between two consecutive Ramsey $\pi/2$ microwave pulses dur-

ing the ground test procedure. Extending the time interval between two microwave pulses will rapidly decrease the number of atoms due to the influence of gravity.

By modulating the microwave frequency on both sides of the Ramsey central peak and locking it to the central peak, the space cold atom microwave clock with this physics package outputs a 100 MHz signal that follows the clock transition frequency. Comparing the frequency of the 100 MHz output signal with a hydrogen maser output, we found that the Alain deviation of the frequency difference is approximately $1.2\times10^{-12}\ \tau^{-1/2}$, which reaches 7×10^{-15} at an average time of 40000 s, as depicted in Fig. 5(b). The short-term stability of the atomic clock is predominantly constrained by the Dick effect and technical noise. Operating in a microgravity environment will increase the duty cycle of the microwave, thereby mitigating the impact of the Dick effect while maintaining the signal-to-noise ratio of technical noise, which will significantly enhance the short-term stability of the atomic clock. The medium and short-term frequency stability of the atomic clock validates the viability of the intracavity cooling scheme. However, its long-term performance depends on factors such as optical stability and system temperature.

4. Conclusion and perspectives

In conclusion, we have presented a physics package based on intracavity laser cooling for a space cold atom clock and have demonstrated the scheme of the cold atomic beam, cooling laser beams, probe laser beam, and microwave coupling around the microwave cavity required for intracavity cooling. The ground-test results showed that more than 5×10^7 cold atoms are captured in the center of the microwave cavity at temperatures of about 5 μK. By locking the microwave frequency on the center of the 12.5 Hz linewidth Ramsey fringes, the cold atom microwave clock with the physics package achieved frequency stability of $1.2\times10^{-12}\ \tau^{-1/2}$. Considering that the cold atom clock operates under microgravity in space, the extension of interrogation time between atoms and microwave would compress the Ramsey linewidth to narrower than 1 Hz. Extending interrogation time will also give rise to the loss of atoms number. According to the ideal atomic cloud expansion analysis, after 1000 ms expansion, the number of the atoms is still 2×10^5, indicating that the noise caused by quantum projection noise is still smaller than that caused by the detection system and Dick effect. We anticipate that the cold atom microwave clock integrated with this physics package will yield a performance enhancement of approximately an order of magnitude in frequency stability at Ramsey linewidth of 0.5 Hz during orbital operation. The intracavity cooling physics package proposed in this paper presents significant potential for miniaturization and lightweight applications. It also enhances the clock's performance by reducing the waste of clock cycles and atomic number loss, which are crucial for the miniaturization research of high-performance atomic clocks in space. Additionally, it contributes to the application of these high-performance atomic clocks in fundamental physics research, deep space exploration, and global navigation and positioning.

Acknowledgments

Project supported by the Space Application System of China Manned Space Program and the Youth Innovation Promotion Association, CAS.

References

[1] Safronova M S, Budker D, DeMille D, Derek F, Kimball J, Derevianko A and Clark C W 2018 *Rev. Mod. Phys.* **90** 025008
[2] Lämmerzahl C, Ahlers G, Ashby N, Barmatz M, Biermann P L, Dittus H, Dohm V, Duncan R, Gibble K, Lipa J, Lockerbie N, Mulders N and Salomon C 2004 *Gen. Relat. Gravit.* **36** 3
[3] Burt E A, Prestage J D, Tjoelker R L, Enzer D G, Kuang D, Murphy D W, Robison D E, Seubert J M, Wang R T and Ely T A 2021 *Nature* **595** 43
[4] Batori E, Almat N, Affolderbach C and Mileti G 2021 *Adv. Space Res.* **68** 4723
[5] Arias E F, Matsakis D, Quinn T J and Tavella P 2018 *IEEE Trans. Ultrason. Ferroelect. Freq. Contr.* **65** 898
[6] Guinot B and Arias E F 2005 *Metrologia* **42** S20
[7] Liu L, Lü D S, Chen W B, *et al.* 2018 *Nat. Commun.* **9** 2760
[8] Lü D S, Ren W, Sun Y, Li T, Qu Q Z, Wang B, Li L, Zhao J B, Zhao X, Ji J W, Ye M F, Xiang J F, Chen W B, Wang Y Z and Liu L 2023 *Natl. Sci. Rev.* **10** nwac180
[9] Ren W, Li T, Qu Q Z, Wang B, Li L, Lü D S, Chen W B and Liu L 2020 *Natl. Sci. Rev.* **7** 12
[10] Laurent P, Massonnet D, Cacciapuoti L and Salomon C 2015 *Comptes Rendus. Phys.* **16** 540
[11] Cacciapuoti L, Armano M, Much R, et al. 2020 *Eur. Phys. J. D* **74** 164
[12] Alonso I, Alpigiani C, Altschul B, et al. 2022 *Epj Quantum. Technol.* **9** 30
[13] Lu Z T, Corwin K L, Renn M J, Anderson M H, Cornell E A and Wieman C E 1996 *Phys. Rev. Lett.* **77** 16
[14] Weiss D S, Riis E, Shevy Y, Ungar P J and Chu S 1989 *J. Opt. Soc. Am. B* **6** 11
[15] Wynands R and Weyers S 2005 *Metrologia* **42** S64
[16] Lü D S, Peng X K, Ren W, Qu Q Z, Li T and Liu L 2017 *Proceedings of the Joint Conference of the European Frequency and Time Forum and IEEE International Frequency Control Symposium (EFTF/IFCS)* July 9–13, 2017, Besancon, France p. 623
[17] Liu P, Meng Y L, Wan J Y, Wang X M, Wang Y N, Xiao L, Cheng H D and Liu L 2015 *Phys. Rev. A* **92** 062101
[18] Esnault F X, Holleville D, Rossetto N, Guerandel S and Dimarcq N 2010 *Phys. Rev. A* **82** 033436
[19] Müller S T, Magalhães D V, Alves R F and Bagnato V S 2011 *J. Opt. Soc. Am. B* **28** 2592
[20] Lee S, Choi G W, Hong H G, Kwon T Y, Lee S B, Heo M S and Park S E 2021 *Appl. Phys. Lett.* **119** 064002
[21] Raab E L, Prentiss M, Cable A, Chu S and Pritchard D E 1987 *Phys. Rev. Lett.* **59** 2631
[22] Ren W, Xiang J F, Zhang Y T, Wang B, Qu Q Z, Zhao J B, Ye M F, Lü D S and Liu L 2015 *Vacuum* **116** 54
[23] Li R X and Gibble K 2004 *Metrologia* **41** 376
[24] Li R X and Gibble K 2010 *Metrologia* **47** 534
[25] Santarelli G, Laurent P, Lemonde P, Clairon A, Mann A G, Chang S, Luiten A N and Salomon C 1999 *Phys. Rev. Lett.* **82** 4619
[26] Santarelli G, Audoin C, Makdissi A, Laurent P, Dick G J and Clairon A 1998 *IEEE Trans. Ultrason. Ferroelect. Freq. Contr.* **45** 4